0026-895X/07/7204-838–849
MOLECULAR PHARMACOLOGY
U.S. Government work not protected by U.S. copyright
Mol Pharmacol 72:838–849, 2007

Vol. 72, No. 4
35527/3252694
Printed in U.S.A.

Structural Determinates for Apolipoprotein E-Derived Peptide Interaction with the α7 Nicotinic Acetylcholine Receptor[S]

Elaine A. Gay, Rachelle J. Bienstock, Patricia W. Lamb, and Jerrel L. Yakel

Laboratory of Neurobiology (E.A.G., P.W.L., J.L.Y.), Scientific Computing Laboratory (R.J.B.), National Institute of Environmental Health Sciences, National Institutes of Health, Department of Health and Human Services, Research Triangle Park, North Carolina

Received February 26, 2007; accepted July 3, 2007

ABSTRACT

Neuronal nicotinic acetylcholine receptor (nAChR) signaling has been implicated in a variety of normal central nervous system (CNS) functions as well as an array of neuropathologies. Previous studies have demonstrated both neurotoxic and neuroprotective actions of peptides derived from apolipoprotein E (apoE). It has been discovered that apoE-derived peptides inhibit native and recombinant α7-containing nAChRs, indicating a direct interaction between apoE peptides and nAChRs. To probe the structure/function interaction between α7 nAChRs and the apoE peptide apoE$_{141–148}$, experiments were conducted in *Xenopus laevis* oocytes expressing wild-type and mutated nAChRs. Mutation of Trp55 to alanine blocks apoE peptide-induced inhibition of acetylcholine (ACh)-mediated α7 nAChR responses. Additional mutations at Trp55 suggest that hydrophobic interactions between the receptor and apoE$_{141–148}$ are essential for inhibition of α7 nAChR function. A mutated apoE peptide also demonstrated decreased inhibition at α7-W55A nAChRs as well as activity-dependent inhibition of both wild-type α7 nAChRs and α7-W55A receptors. Finally, a three-dimensional model of the α7 nAChR was developed based on the recently refined *Torpedo marmorata* nACh receptor. A structural model is proposed for the binding of apoE$_{141–148}$ to the α7 nAChR where the peptide binds at the interface between two subunits, near the ACh binding site. Similar to the functional data, the computational docking suggests the importance of hydrophobic interactions between the α7 nAChR and the apoE peptide for inhibition of receptor function. The current data suggest a mode for apoE peptide binding that directly blocks α7 nAChR activity and consequently may disrupt nAChR signaling.

Neuronal nicotinic acetylcholine receptors (nAChRs) are members of the Cys-loop ligand-gated ion channel superfamily. These receptors are found throughout the central (CNS) and peripheral nervous systems and are involved in a variety of normal brain functions, including cognitive tasks, neuronal development, and mediating the rewarding effects of nicotine (Jones et al., 1999). The nAChRs are expressed both pre- and postsynaptically, where they influence neuronal signaling (for review, see Berg and Conroy, 2002) and are therefore a significant therapeutic target for many neurodegenerative, neurological, and psychiatric disorders such as Alzheimer's disease, Parkinson's disease, epilepsy, and schizophrenia (for review, see Levin, 2002; Picciotto and Zoli, 2002; Raggenbass and Bertrand, 2002).

The nAChRs are pentameric cationic channels in which each subunit has a large extracellular domain, four α helical bundles that traverse the cellular membrane, and one intracellular α helix. In the rodent CNS, nAChRs are either heteromeric (consisting of both α and β subunits) or homomeric (α subunits only; e.g., α7). nAChRs are often considered allosteric proteins because the acetylcholine (ACh) binding site is within the N-terminal domain at the interface between two subunits (principal and complimentary), and some 60 Å from the pore region, where the channel gates and allows the flow of ions through the membrane. Over time, the ligand binding pocket of the nAChR has been defined through a variety of techniques including NMR, site-directed mutagenesis, and kinetic and pharmacological analysis (for review, see Sine, 2002). However, our understanding of the structure and function of the ligand binding pocket of nAChRs has expanded recently because of the solution of several high resolution crystal structures of the ACh binding protein (AChBP; a homolog of the nAChR extracellular domain) from *Lymnaea stagnalis*, *Aplysia californica,* and *Bulinus truncatus* (Brejc et al., 2001; Celie et al., 2005a,b) and the cryoelec-

This research was supported by the Intramural Research Program of the National Institutes of Health.

Article, publication date, and citation information can be found at http://molpharm.aspetjournals.org.

doi:10.1124/mol.107.035527.

[S] The online version of this article (available at http://molpharm.aspetjournals.org) contains supplemental material.

ABBREVIATIONS: nAChR, nicotinic acetylcholine receptor; CNS, central nervous system; ACh, acetylcholine; apoE, apolipoprotein E; MLA, methyllycaconitine; α-BgTx, α-bungarotoxin; PDB, Protein Data Bank; RMS, root-mean-square; AChBP, acetylcholine binding protein.

tron microscopy structure of the *Torpedo marmorata* nAChR (Unwin, 2005). A variety of small peptide toxins act as nAChR antagonists; for instance, several snake and cone snail toxins are pharmacologically selective for the different nAChRs. Recent crystal structures of the AChBP with different toxins reveal that these peptides bind at the interface between two subunits (Celie et al., 2005a; Hansen et al., 2006; Ulens et al., 2006).

Apolipoprotein E (apoE) has traditionally been studied for its role in lipid metabolism and cholesterol transport. More recently, the inheritance of particular apoE isoforms has been identified as a risk factor in a variety of pathological conditions of the CNS, including Alzheimer's disease and Parkinson's disease. The apoE protein has two domains, a receptor-binding N-terminal domain and a lipid-binding C-terminal domain, with a thrombin cleavage site separating these two domains. Proteolytic fragments of apoE have been shown to be increased in the brain of patients with Alzheimer's disease (Marques et al., 1996), whereas some synthetic peptides of apoE have been shown to have neurotoxic effects (Clay et al., 1995; Tolar et al., 1997). In contrast, apoE mimetic peptides from the receptor-binding domain have recently demonstrated a potential therapeutic usefulness in a variety of CNS injury models involving inflammation. After both head trauma and ischemic injury in rodents, administration of apoE peptides improved cognitive recovery (Lynch et al., 2005; McAdoo et al., 2005). In addition, treatment with apoE mimetic peptides reduces the clinical symptoms of experimental autoimmune encephalomyelitis, an animal model of multiple sclerosis, as well as reducing demyelination and inflammation (Li et al., 2006). We have demonstrated that apoE-derived peptides can inhibit nAChRs expressed on interneurons in rat hippocampal slices, as well as α7 receptors expressed in *Xenopus laevis* oocytes, indicating a possible direct interaction between apoE and nAChRs (Klein and Yakel, 2004; Gay et al., 2006).

To understand the binding interaction between apoE-derived peptides and the α7 nAChR on a molecular level, we used a combination of binding experiments, site-directed mutagenesis of the α7 nAChR, electrophysiological recordings, and molecular modeling. Point mutations were made in nAChR amino acids that line the interface between subunits. Mutant α7 nAChRs were characterized using two-electrode voltage-clamp in *X. laevis* oocytes. The ability of various apoE peptides to inhibit the different mutant receptors was tested. Finally, a three-dimensional molecular model of the α7 nAChR was developed based on the recently refined 4-Å *T. marmorata* ACh receptor structure (Unwin, 2005). ApoE peptides were docked within the computational model, and the results were used to suggest a possible interaction between the apoE peptide and the nAChR that corresponds with the functional data. The current data suggest a mode for apoE peptide binding that directly blocks α7 nAChR activity and consequently disrupts nAChR signaling.

Materials and Methods

Peptide Synthesis. ApoE-derived peptides were synthesized by Sigma-Genosys (The Woodlands, TX) at a purity of 95% and reconstituted in either sterile, deionized water or dimethyl sulfoxide yielding stock concentrations of 15 mM. Stock solutions were stored at −20°C and diluted to desired concentrations on the day of the experiment. The peptides used in this study were acetylated at the amino terminus and amide-capped at the carboxyl terminus.

Oocyte Preparation. Female *X. laevis* frogs were anesthetized in ice-cold water containing 0.3% Tricaine methanesulfonate. Oocytes were dissected and defolliculated by treatment with collagenase B (2 mg/ml; Roche Diagnostics, Indianapolis, IN) and trypsin inhibitor (1 mg/ml; Invitrogen, Carlsbad, CA) for 2 h. Primers were designed containing the desired mutations in the α7 nAChR. Mutations were made in the α7 nAChR DNA as directed using the QuikChange II XL site-directed mutagenesis kit (Stratagene, La Jolla, CA). The T7 mMessage mMachine kit (Ambion, Austin, TX) was used to prepare capped RNA from the mutated plasmid linearized using XbaI. The total amount of RNA injected for α7 nAChR subunits and mutant α7 nAChRs was ~75 ng for binding experiments and ~50 ng for functional experiments.

^{125}I-α-Bungarotoxin Competition Binding. For binding assays, oocytes injected with wild-type α7 nAChRs were incubated for 30 min with various concentrations of either $apoE_{141–148}$ or methyllycaconitine (MLA) in bath solution (96 mM NaCl, 2 mM KCl, 1.8 mM $CaCl_2$, 1 mM $MgCl_2$, and 5 mM HEPES) plus 1 mg/ml bovine serum albumin. After the addition of 5 nM ^{125}I-α-bungarotoxin (α-BgTx), oocytes were incubated at room temperature with shaking for 1 h. The reaction was stopped by washing oocytes three times with bath solution. Each condition was run in triplicate, and oocytes were counted individually. Bound ^{125}I-α-BgTx was measured by gamma-counting. Nonspecific binding was determined in the presence of 1 μM MLA and was similar to binding in oocytes not injected with the α7 nAChR.

Oocyte Electrophysiology. Current responses were obtained by two-electrode voltage-clamp recording at a holding potential of −60 mV using a Geneclamp 500 and pClamp 8 software (Molecular Devices, Sunnyvale, CA). Electrodes contained 3 M KCl and had a resistance of <1 MΩ. ACh and peptides were prepared daily in bath solution (96 mM NaCl, 2 mM KCl, 1.8 mM $CaCl_2$, 1 mM $MgCl_2$, and 5 mM HEPES) from frozen stocks. ACh was applied for various periods using a synthetic quartz perfusion tube (0.7 mm i.d.) operated by a computer-controlled valve. Peptides were bath applied. Data were analyzed using pClamp 8, Excel (Microsoft, Redmond, WA), and Prism 4 (GraphPad Software, San Diego, CA). Data for ACh dose-response curves were normalized to the peak current response at 1 or 10 mM ACh for each receptor mutant. Peak current responses to each dose of ACh were averaged, and then the mean ± S.E.M were analyzed by nonlinear regression using a logistic equation (Prism 4). ACh EC_{50} values were compared using a two-tailed *t* test with a Bonferroni correction for α inflation. Activity dependence of apoE peptide block was tested as follows: ACh was rapidly applied (250–500 ms) every 2 min to obtain control data, then apoE peptide was bath-applied for 10 min in the absence of ACh stimulation. Finally, in the continued presence of apoE peptide, ACh was again rapidly applied every 2 min for up to 10 min. The peak ACh current response was compared among 1) control, 2) the first rapid application of ACh after apoE peptide (10 min) bath application and 3) after 10 min of apoE peptide and repetitive ACh application (this was considered maximal inhibition). Multiple group comparisons were performed by one-way analysis of variance followed by a Dunnett's multiple comparison test to make specific comparisons between individual values (Prism 4).

Development of the Rat α7 Model. A molecular model of the complete rat α7 nAChR, including the extracellular, intracellular, and transmembrane domains, was developed based on the solved 4-Å resolution experimental *T. marmorata* nAChR structure (PDB code 2BG9, Unwin, 2005). The model was developed based on the sequence alignment shown in supplemental Fig. 1. The α chain of the *T. marmorata* nAChR shares 43% identity and 65% similarity with the rat α7 protein sequence. The model of a single chain was developed using Prime v. 1.5 (Schrodinger LLC, New York, NY) protein homology modeling software package. The model for the complete pentameric structure was constructed from the single chain coordi-

nates and the symmetry relationship between the monomers as in the solved *T. marmorata* nAChR structure. The quality of the model structure was verified using ProCheck (Morris et al., 1992; Laskowski et al., 1993), examining the Ramachandran plot, and comparing the rat α7 model structure with the original *Torpedo* structure (PDB code 2BG9), with the AChBP structure (PDB code 1UW6; Celie et al., 2004) and with other model structures (Le Novère et al., 2002).

Docking Studies. The starting α-helical structures of the apoE peptides used for computational docking were taken from the structure of this peptide segment in the intact apoE protein (PDB code 1GS9; Segelke et al., 2000). A fragment of the complete model consisting of a dimer model of two extracellular subunits of the α7 nAChR was used for the docking studies to constrain the computational problem to a reasonable time limit. Peptides were docked using a dimer corresponding to the α and β subunits of the *T. marmorata* nAChR. Peptides were docked using the ZDOCKpro program (Accelrys, San Diego, CA) (Chen et al., 2003; Li et al., 2003) consisting of a two-phase docking procedure. The ZDOCK/RDOCK method has been validated by multiple independent protein-protein docking studies and has been found to be a reliable method for the prediction of protein-protein interactions (Wiehe et al., 2005). The program ZDOCK initially identifies the docking positions possible within the receptor for the peptides based on shape, steric, and electrostatic complementarities. Once docking positions are identified, they are ranked and refined by the second program, RDOCK, which is based on the CHARMM forcefield and calculates the energetics between the protein and docked peptides and ranks the docked poses. RDOCK calculations were performed on the top 5000 ZDOCK-docked structures. The top RDOCK results were clustered to identify and characterize the top potential peptide binding sites. However, because the ZDOCKpro program was not parameterized to handle acetylated and amidated peptides, the docked peptides from the top RDOCK poses that were missing N-terminal acetylation and C-terminal amidation had these termini added. The peptide/protein system with amidation and acetylation was then minimized using the CHARMM forcefield, and the system was subjected to limited molecular dynamics to remove bad contacts and then reminimized. The same treatment and conditions were applied for docking each of the apoE peptides, as well as docking $apoE_{141–148}$ with the α7-W55A nAChR mutant.

Results

Competition Binding between α-Bungarotoxin and $apoE_{141–148}$. Previous studies indicated that a synthetic apoE peptide, containing the low-density lipoprotein receptor binding region, can inhibit α7 nAChR-mediated ACh-induced currents through a direct interaction. In addition, previous functional data suggest that this peptide/receptor interaction is noncompetitive with α-BgTx blockade and possibly ACh gating of the receptor (Gay et al., 2006). Direct binding experiments using α-BgTx were carried out to determine whether $apoE_{141–148}$ binds competitively with the toxin. Increasing concentrations of $apoE_{141–148}$ did not compete for the binding of ^{125}I-α-BgTx, whereas MLA was able to dose-dependently block ^{125}I-α-BgTx binding to α7 nAChRs expressed in *X. laevis* oocytes ($K_{0.5}$ = 1.8 ± 0.6 nM, Hill slope = 0.91 ± 0.13, n = 3; Fig. 1).

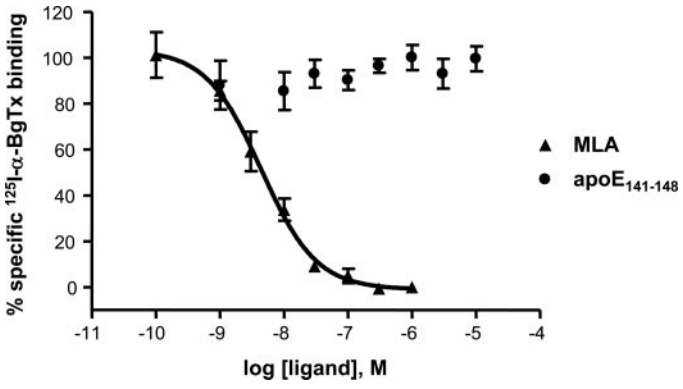

Fig. 1. $ApoE_{141–148}$ does not compete for ^{125}I-α-bungarotoxin binding. $ApoE_{141–148}$ was unable to inhibit the initial rate of ^{125}I-α-BgTx binding to α7 nAChRs expressed in *X. laevis* oocytes. In contrast, MLA blocked ^{125}I-α-BgTx binding in a concentration dependent manner. Each data point represents the mean ± S.E.M. of three to four experiments conducted in triplicate. The MLA curve was generated by nonlinear regression using a logistic equation with variable slope.

Inhibition of Mutant α7 nAChRs by apoE-Derived Peptides. Various point mutations in amino acids that line the interface between subunits of the α7 nAChR were generated. These were expressed in *X. laevis* oocytes, and α7 nAChR-mediated responses were elicited by application of ACh to generate dose-response curves for each mutant receptor that functionally expressed (Table 1). All mutations except E19A, G152A, E189D, and K192A demonstrated a significantly different EC_{50} value compared with wild type. Several mutant receptors that we generated were not functional, including N16A, E19K, D25K, W67A, W67T, D89A, D89K, D97A, Y188A, E193A, E193K, Y195A, and Y195T.

As previously reported (Gay et al., 2006), the eight-amino-acid peptide $apoE_{141–148}$ (3 μM, near maximal inhibition) significantly reduced the amplitude of wild-type α7 nAChR-mediated responses by 78 ± 3% (Table 1, Fig. 2A). It is noteworthy that $apoE_{141–148}$ had a dramatically decreased ability to inhibit only the α7-W55A mutant nAChR (inhibition = 10 ± 2%, Table 1, Fig. 2B), whereas the inhibition of the other functional mutant receptors was not considerably reduced (Table 1, Fig. 2C). In addition, the longer 17 amino acid fragment, $apoE_{133–149}$, also demonstrated a significantly decreased inhibition of ACh-induced responses at the α7-W55A mutant receptor (51 ± 15%; n = 6), although this block of inhibition was less than for the shorter $apoE_{141–148}$ peptide.

Additional mutations were made at position 55 of the α7 nAChR to probe the chemical and structural requirements of this W residue for the interaction between $apoE_{141–148}$ and the receptor. The Trp at position 55 was also mutated to Cys, Val, Tyr, Phe, Leu, Thr, and Arg. The Trp-to-Leu, -Thr, and -Arg mutations were nonfunctional. For the rest, the ability of the $apoE_{141–148}$ peptide to block these mutant receptors was similar to wild-type α7 receptors (Fig. 3A). Dose-response curves were generated, and both the α7-W55A and α7-W55Y receptors displayed an increased potency for ACh (compared with wild type), whereas the α7-W55V and α7-W55C receptors displayed a decreased ACh potency (Fig. 3B, Table 1).

Activity-Dependent Block of Modified $apoE_{141–148}$ Peptide. It had been demonstrated (Gay et al., 2006) that when the two positively charged lysines (at positions 143 and 146) of $apoE_{141–148}$ were substituted with leucines (which will be referred to as $apoE_{141–148}$2K/2L), this new peptide was able to inhibit ACh-induced current responses similarly to $apoE_{141–148}$. However, this change dramatically decreased the rate of block (Gay et al., 2006). In the current study, we tested the ability of $apoE_{141–148}$2K/2L to inhibit the α7-W55A nAChR. $ApoE_{141–148}$2K/2L (3 μM) showed a significantly decreased ability to block ACh-mediated responses at the α7-W55A nAChR (inhibition = 26 ± 7%, n = 9) compared with

the wild-type α7 nAChR (inhibition = 70 ± 3%, n = 9, Fig. 4A&B).

Based on the earlier data showing a decreased rate of block with apoE$_{141–148}$2K/2L, the activity dependence of this peptide was tested at both the wild-type α7 nAChR and the mutant α7-W55A nAChR (see *Materials and Methods*). For the wild-type α7 nAChR, the first application of ACh after bath application of apoE$_{141–148}$2K/2L for 10 min had an average inhibition of 18 ± 2% compared with maximal inhibition after 10 min of repetitive ACh application of 67 ± 10% (n = 4). Therefore, 76% of the maximal inhibition of 3 μM apoE$_{141–148}$2K/2L at α7 nAChRs was activity-dependent (i.e., was not present without activation of the channel). The average inhibition for apoE$_{141–148}$ was 77 ± 4% after 10-min bath application (n = 5, data not shown). At the α7-W55A nAChR, the first application of ACh after bath application of apoE$_{141–148}$2K/2L had an average inhibition of 2 ± 1% compared with maximal inhibition after repetitive ACh application of 31 ± 8% (n = 4). Compared with wild-type α7 receptors, inhibition of α7-W55A nAChRs by apoE$_{141–148}$2K/2L (3 μM) was 94% activity-dependent (Fig. 4, C and D). In addition, the voltage-dependence of the apoE$_{141–148}$2K/2L peptide was tested. The ability of apoE$_{141–148}$2K/2L to inhibit α7-mediated ACh responses was not significantly different at holding potentials of −60 mV versus +30 mV (inhibition = 63 ± 2%, n = 10, Fig. 4E).

Modeling. A molecular model of the rat α7 nAChR was developed to suggest potential interactions between apoE peptides and the rat α7 nAChR (Fig. 5). The quality of the α7 nAChR model was verified using a variety of methods. The ProCheck validation gave the structure an overall final Gfactor score well above −0.50. The Ramachandran plot illustrated that the majority of residues fall within permitted regions; 97.4% of the residues were in the most favored and allowed regions. Only 4 residues were in disallowed regions (0.7%), and those were near the amino and carboxyl termini and not near the region of interest for probing docking interactions. The ProStat Structure Check

TABLE 1

Characterization of mutant α7 nAChRs expressed in *X. laevis* oocytes

Columns correspond to the mutated amino acid residue, whether the mutated receptor was functional (i.e., could be activated by ACh), the EC$_{50}$ value, the Hill slope, the ratio between the mutant's EC$_{50}$ and the wild-type receptor's EC$_{50}$ values, and the ability of apoE$_{141–148}$ to block the function of the mutated receptor. Each particular mutation is listed as the wild-type amino acid, the amino acid position number, followed by the amino acid residue to which the mutant was converted. Data for percentage block of apoE$_{141–148}$ are presented as the mean ± S.E.M. with the number of oocytes in parenthesis. The percentage block by apoE$_{141–148}$ is for a single concentration of 3 μM.

Mutation	Functional	EC$_{50}$ (95% CI)	Hill slope	EC$_{50}$mut/EC$_{50}$wt	Block apoE$_{141–148}$
		μM			*% (n)*
α7 wt	Yes	120 (104–138)[a]	1.7 ± 0.2[a]	1	78 ± 3 (13)
Y8A	Yes	171 (149–196)	2.3 ± 0.2	1.4	81 ± 2 (5)
N16A	No				
E19A	Yes	117 (95–143)	1.6 ± 0.2	0.97	73 ± 3 (6)
E19K	No				
D25A	Yes	N.D.			71 ± 7 (3)
D25K	No				
S34A	Yes	240 (220–261)	2.2 ± 0.2	2	76 ± 3 (6)
D42A	Yes	346 (239–499)	0.91 ± 0.1	2.9	84 ± 3 (2)
N47A	Yes	430 (380–486)	1.8 ± 0.2	3.6	78 ± 2 (3)
W55A	Yes	58 (49–68)[a]	3.1 ± 0.6[a]	0.5	11 ± 2 (14)
W55C	Yes	315 (260–382)[a]	2.1 ± 0.4[a]	2.6	81 ± 2 (3)
W55R	No				
W55T	No				
W55L	No				
W55V	Yes	203 (185–223)[a]	2.3 ± 0.2[a]	1.7	74 ± 4 (6)
W55Y	Yes	51 (43–60)[a]	2.5 ± 0.4[a]	0.4	80 ± 2 (7)
W55F	Yes	134 (98–184)[a]	1.7 ± 0.4[a]	1.1	84 ± 1 (5)
Y64A	Yes	76 (70–82)	4.1 ± 0.8	0.6	78 ± 3 (6)
W67A	No				
W67T	No				
D89A	No				
D89K	No				
D97A	No				
T106A	Yes	183 (162–207)	2.6 ± 0.3	1.5	81 ± 1 (5)
W149A	Yes	724 (625–839)	2.2 ± 0.4	6.0	79 ± 3 (3)
W149T	Yes	N.D.			78 ± 3 (4)
S150A	Yes	215 (194–237)	2.1 ± 0.2	1.8	80 ± 3 (4)
Y151A		N.D.			87 ± 1 (4)
Y151T	Yes	58 (48–71)	1.5 ± 0.2	0.5	82 ± 2 (6)
G152A	Yes	105 (89–125)	2.1 ± 0.5	0.9	84 ± 3 (3)
E162A	Yes	N.D.			89 ± 1 (5)
K186A	Yes	N.D.			82 ± 4 (3)
F187A	Yes	177 (145–216)	1.1 ± 0.1	1.5	89 ± 2 (4)
F187L	Yes	44 (33–59)	0.97 ± 0.1	0.4	78 ± 2 (8)
Y188A	No				
E189A	Yes	54 (50–60)	2.7 ± 0.3	0.5	89 ± 2 (6)
E189D	Yes	138 (124–154)	1.8 ± 0.1	1.2	79 ± 4 (7)
K192A	Yes	121 (107–137)	1.8 ± 0.2	1.0	80 ± 2 (4)
E193A/K	No				
Y195A/T	No				

CI, confidence interval; mut, mutation; wt, wild-type; N.D., not determined.
[a] These data are presented in E. A. Gay, R. Giniatullin, A. Skorinkin, and J. Yakel, submitted.

program within the Accelrys software identified no bad contacts within the model structure.

The RMS deviations between the model structure developed and other experimentally solved structures, as well as hydrogen bonding pattern around the active site of the model and other experimentally similar structures, compared favorably. Within the identified apoE$_{141–148}$ binding site from our docking computations, our rat α7 model had seven hydrogen bonds, five of which were identical to the hydrogen bonds found in the *T. marmorata* nAChR, and five of which were identical to the AChBP structure (PDB code 1UW6; Celie et al., 2004). Comparison of the complete rat α7 model developed with the original *T. marmorata* nAChR (PDB code 2BG9; Unwin, 2005) yielded an RMS deviation from a DALI (Holm and Sander, 1995; Holm and Park, 2000) structural comparison and overlay of 362 aligned Cα residues = 0.60 Å. A comparison with the published model of the chick α7 nAChR yielded an RMS deviation = 3.2 Å (Le Novère et al., 2002). There is 80% sequence identity between the rat and chick α7 nAChR over the 194 aligned residues of the extracellular domain.

Because our model is based on the *T. marmorata* nAChR structure, it has the C-loop in the open configuration (Fig. 5A), which is probably equivalent to the closed/resting state of the nAChR (Dutertre and Lewis, 2006). It was noted in the *T. marmorata* nAChR structure that all the monomers are not conformationally equivalent with respect to their twist and orientation relative to the central axis (Unwin, 2005). Our model is consistent with this structure and preserves the asymmetry in packing between the monomeric subunits.

The rotations in the α subunits of the *T. marmorata* nAChR have been described as "distorted" conformations, which convert to nondistorted conformations upon ligand binding and channel opening (Unwin, 2005). It is important to note that the modeling data presented here represents the interaction of apoE peptides at one of five possible interfaces.

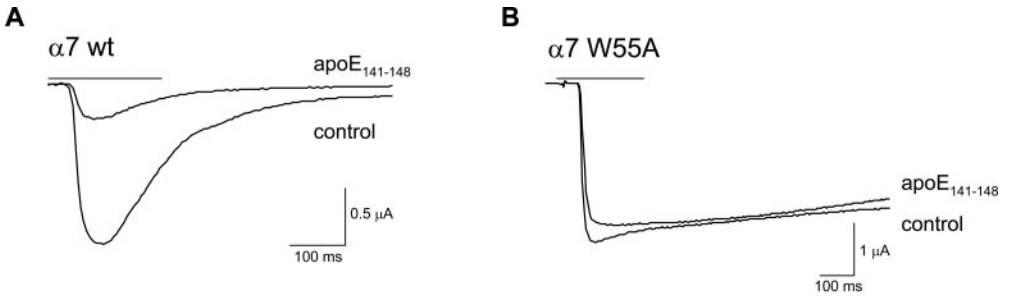

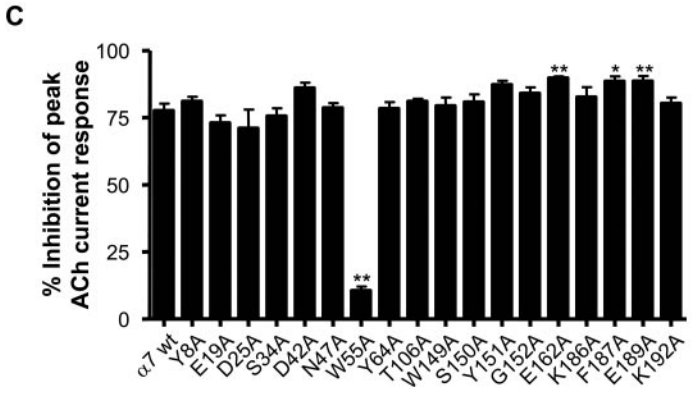

Fig. 2. ApoE$_{141–148}$ inhibits α7 nAChRs except for the α7-W55A mutant. A, the α7 nAChR-mediated responses were elicited by application of 1 mM ACh for 250 to 500 ms (bar) at 2-min intervals. Representative traces for ACh-evoked current responses before and during bath application of apoE$_{141–148}$ are illustrated for wild-type α7 (A) and mutant α7-W55A (B). Peak ACh current responses returned with washout of the peptide. C, ApoE$_{141–148}$ (3 μM) produced marked inhibition of wild-type and all mutant α7 nAChRs tested except at α7-W55A. Data are the mean ± S.E.M. of 3 to 14 oocytes per bar. *, $p < 0.05$, **, $p < 0.01$, one-way analysis of variance, followed by Dunnett's multiple comparison test.

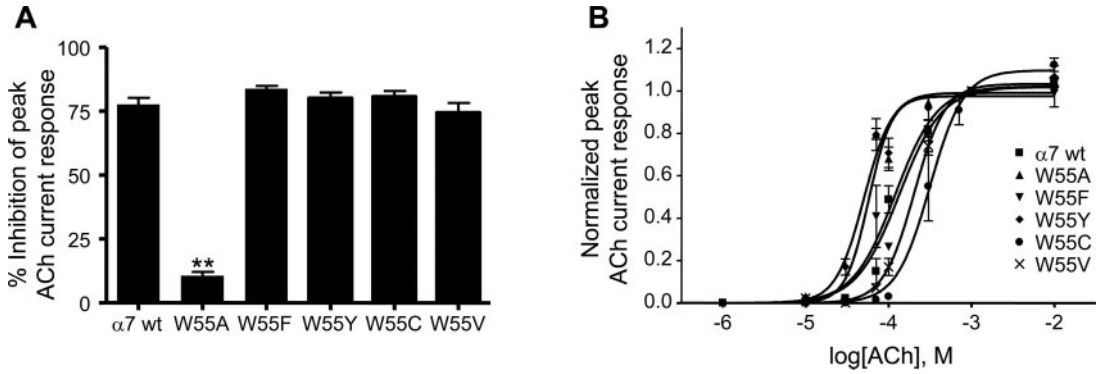

Fig. 3. Additional mutations of Trp55 do not effect apoE$_{141–148}$ block of α7 nAChR. A, changing the amino acid at Trp55 to either Phe, Tyr, Cys, or Val did not significantly decrease apoE$_{141–148}$ inhibition of α7 nAChRs. Data are the mean ± S.E.M. of 3 to 14 oocytes per bar. **, $p < 0.01$, one-way analysis of variance, followed by Dunnett's multiple comparison test. B, mutations of Trp55 to alanine and tyrosine increased the potency of ACh, whereas mutations of Trp55 to cysteine and valine decreased ACh potency. Dose-response curves were generated using nonlinear regression. Data were normalized to the peak current response at 1 mM ACh for each receptor type. Data are the mean ± S.E.M. of 3 to 14 oocytes per point.

It is likely that potential interactions at the other interfaces would include some binding sites similar to those described here, as well as others that are unique for a given interface. Future studies will explore computational docking within the other dimeric interfaces of the homopentameric structure.

$ApoE_{141–148}$, $apoE_{141–148}$2K/2L and an inactive mutated apoE peptide, $apoE_{141–148}$2K/2E (Gay et al., 2006), were computationally docked with the molecular model of the rat α7 nAChR to identify their putative binding site(s) and mode of interaction. $ApoE_{141–148}$ was additionally docked with a model of the α7-W55A nAChR mutant. The top 10 docked poses for $apoE_{141–148}$ with the least energy clustered in several well defined sites (Fig. 6A) classified to be 1) at the level of the C-loop at or near the ligand binding pocket, 2) just above the level of the C-loop on the pore side, and 3) near the α helix at the top of the receptor. The lowest energy docked $apoE_{141–148}$ peptide pose was found at position 2. The second lowest energy docked conformer of $apoE_{141–148}$ was located at position 1 and complemented the experimental results in which the W55A mutation significantly decreased the apoE peptide-receptor interaction. Mutation of amino acids (Asn16, Glu19, Asp25, and Trp67) within position 3 did not affect the ability of $apoE_{141–148}$ to inhibit α7 nAChRs. Those potential docking sites that were not at the interface between two subunits were not considered because they were suspect as a result of the lack of additional subunits that would have created another interface. The lowest energy docked confirmation of $apoE_{141–148}$ at position 1 was used for further evaluation with this model because it corresponded with the functional data suggesting a potential key interaction between Trp55 and the apoE peptide. However, the ability of $apoE_{141–148}$ to interact at other identified sites has not been ruled out.

In the $apoE_{141–148}$-docked model (Fig. 7A), Trp55 of the α7 nAChR was less than 5 Å from each of the three leucine residues (apoE Leu141, Leu144, and Leu148) within the docked peptide, suggesting the major interaction between peptide and receptor may be hydrophobic in nature. In addition, apoE Leu141 is buried in a hydrophobic pocket surrounded by residues Leu35, Trp55, and Leu119 of the α7 nAChR, whereas apoE Leu148 is buried in a hydrophobic pocket surrounded by Trp55, Tyr93, Trp149, Tyr188, and

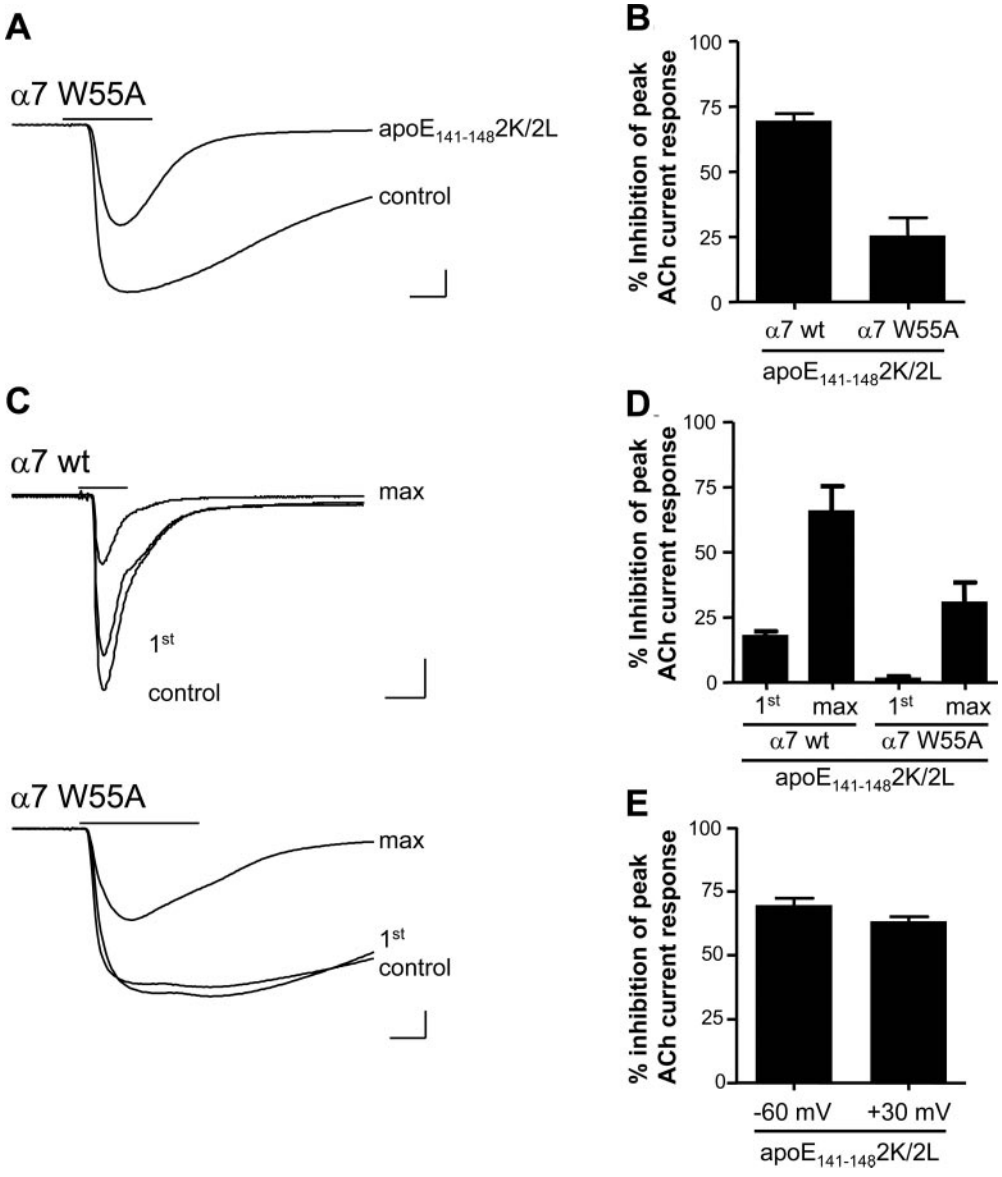

Fig. 4. $ApoE_{141–148}$2K/2L partially blocks the α7-W55A nAChR and demonstrates activity-dependence. A, a representative trace for ACh-evoked current responses before and during bath application of $apoE_{141–148}$2K/2L is illustrated for α7-W55A nAChR. B, $ApoE_{141–148}$2K/2L (3 μM) produced marked inhibition of the wild-type α7 nAChR while only partially inhibiting the mutant α7-W55A receptor. Data are the mean ± S.E.M. of eight to nine oocytes per bar. C, representative traces showing activity-dependent inhibition by $apoE_{141–148}$ 2K/2L at both the wild-type (top) and α7-W55A nAChR (bottom). D, $ApoE_{141–148}$2K/2L (3 μM) demonstrated activity-dependent inhibition at both the wild-type and α7-W55A nAChR. Data are the mean ± S.E.M. of four oocytes per bar. E, the inhibition of α7 nAChR by $apoE_{141–148}$2K/2L is not significantly different at holding potentials of −60 versus +30 mV. Data are the mean ± S.E.M. of 9 to 10 oocytes per bar. Legend bars for traces: A, 1 nA, 100 ms; C, top, 0.5 nA, 200 ms; and bottom, 1 nA, 100 ms.

Tyr195 (Fig. 7C). Hydrogen bonds that stabilize interactions between apoE$_{141–148}$ and the α7 nAChR involve receptor residues Leu37, Leu38, Met160, Glu162, Ser167, and Lys186 (Fig. 7, A and B). The majority of the hydrogen bond interactions with the active peptide occur between the receptor and the apoE Arg145 residue. In addition, upon apoE$_{141–148}$ docking in the model, the tip of the C-loop (Cys191) moves outward from the binding pocket approximately 1.4 Å in a manner similar to that of other known antagonists (Dutertre and Lewis, 2006). All potential molecular interactions between apoE$_{141–148}$ and the α7 nAChR are summarized in Table 2.

Similarly to apoE$_{141–148}$ at the wild-type α7 nAChR, when apoE$_{141–148}$ is docked with the mutant α7-W55A nAChR, the majority of the top 10 conformers with the least energy are clustered at position 1 of the receptor (Fig. 6B). However, in contrast to interactions with the wild-type receptor, apoE$_{141–148}$ loses two of the three predicted hydrophobic interactions with Trp55 when it is mutated to Ala (Fig. 7D). The C-loop also appears less bent away from the ligand-binding pocket. These data suggest a loss of the hydrophobic environment that serves to stabilize the interaction between the peptide and receptor. In the apoE$_{141–148}$ with α7-W55A nAChR docking simulation, hydrophobic interactions are replaced with more hydrophilic interactions, and hydrogen bonds between hydrophilic charged residues in the peptide apoE Arg142, Lys143, Arg145, Lys146, and Arg147 and surrounding receptor residues. With the α7-W55A nAChR, many of these receptor residues can participate in interactions with the peptide that were prevented in the wild-type α7 nAChR by the presence of the larger hydrophobic residue, W55.

When docking simulations were run with the activity dependent apoE$_{141–148}$2K/2L peptide, there was an increase in the spread of peptide conformers at the interface between the ex-

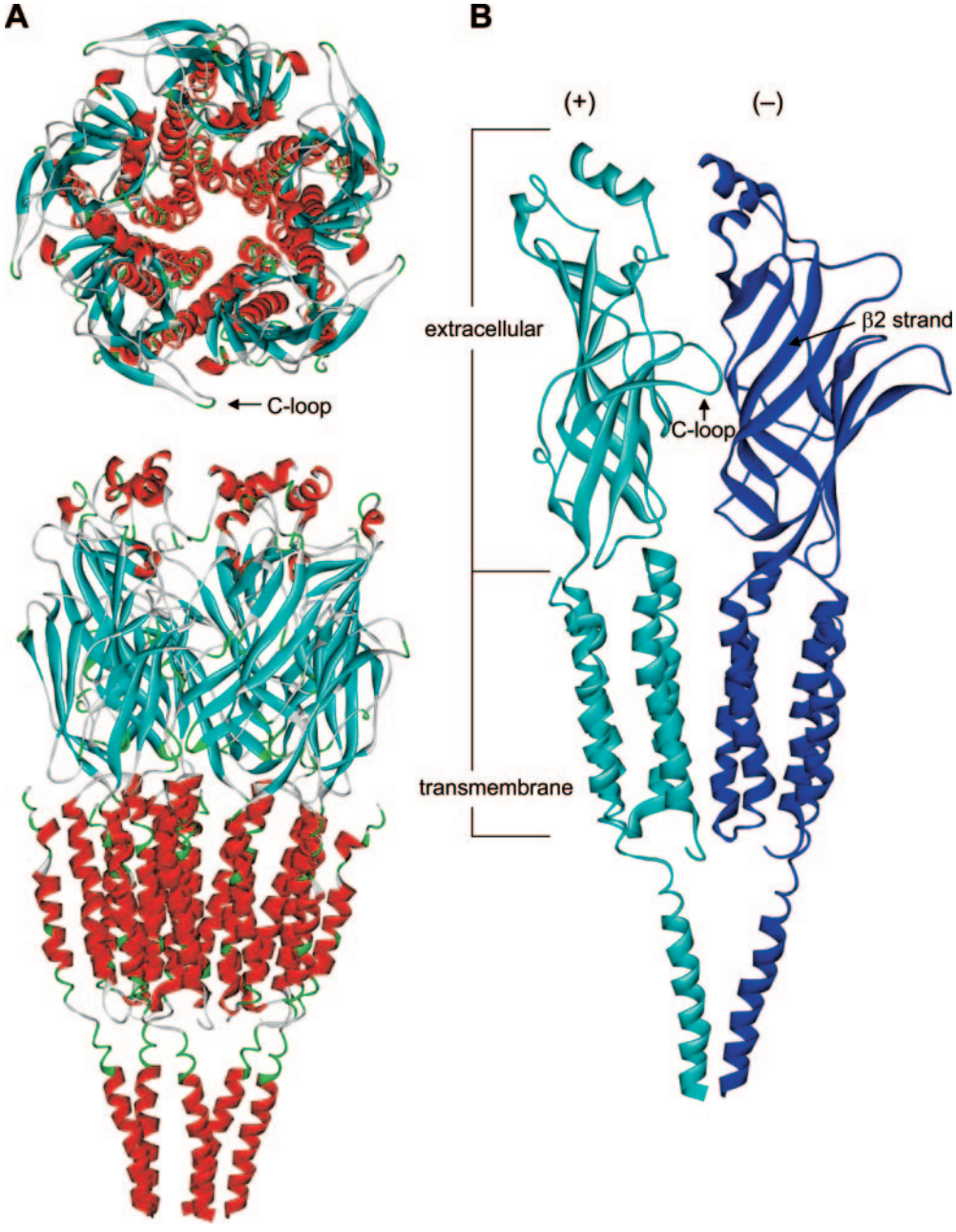

Fig. 5. Molecular model of the rat α7 nAChR. A model was developed based on sequence alignment with the cryo-electron microscopy structure of the *T. marmorata* nAChR (Unwin, 2005). The model of a single chain was developed using Schrodinger Prime followed by construction of the pentameric structure based on the symmetry relationship between monomers. A, both a top-down (top) and side-view (bottom) of the pentameric rat α7 nAChR. Secondary structures are indicated: red, α helix; blue, β strands. B, two subunits of the rat α7 nAChR model with structural features highlighted, +, principal subunit; −, complementary subunit.

tracellular subunits around the C-loop (Fig. 6C). When the lowest energy peptide position most similar to apoE$_{141–148}$ was investigated more thoroughly (first position), it was observed that apoE$_{141–148}$2K/2L preserves two of the three hydrophobic interactions between Trp55 and apoE Leu143 and apoE Leu146. In addition, apoE$_{141–148}$2K/2L has more potential hydrophilic hydrogen bond interactions between the peptide and receptor than apoE$_{141–148}$. Finally, when the inactive apoE$_{141–148}$2K/2E peptide was docked to the α7 nAChR, 50% of the top 10 ranked conformers did not interact at the level of the C-loop at or near the ACh binding site or Trp55 (Fig. 6D). These data are consistent with previous functional results suggesting that this peptide is unable to effectively block α7 nAChR responses in a manner similar to apoE$_{141–148}$.

Discussion

Previous studies have demonstrated that peptides derived from the LDLR binding domain of apoE inhibit α7-containing nAChRs both in hippocampal interneurons, and those expressed in *X. laevis* oocytes (Klein and Yakel, 2004; Gay et al., 2006). In addition, inhibition of ACh-induced current responses at the α7 nAChR is voltage- and activity-independent as well as noncompetitive for α-bungarotoxin and possibly ACh gating of the receptor (Gay et al., 2006). The current study employed direct binding studies, site-directed mutagenesis of the α7 nAChR, mutated apoE peptides, as well as molecular modeling to characterize the binding interaction between apoE$_{141–148}$ and the α7 nAChR responsible for channel inhibition.

When the ability of apoE$_{141–148}$ to inhibit ACh responses at each mutant receptor was tested, only the mutation of Trp55 to Ala blocked apoE$_{141–148}$-mediated inhibition. Inhibition by apoE$_{133–149}$ was partially blocked at the α7-W55A nAChR mutant, suggesting that Trp55 seems critical for inhibition of ACh responses by both apoE peptides. Trp55 of the rat α7 nAChR lies within the β2 strand and is projected to be in or

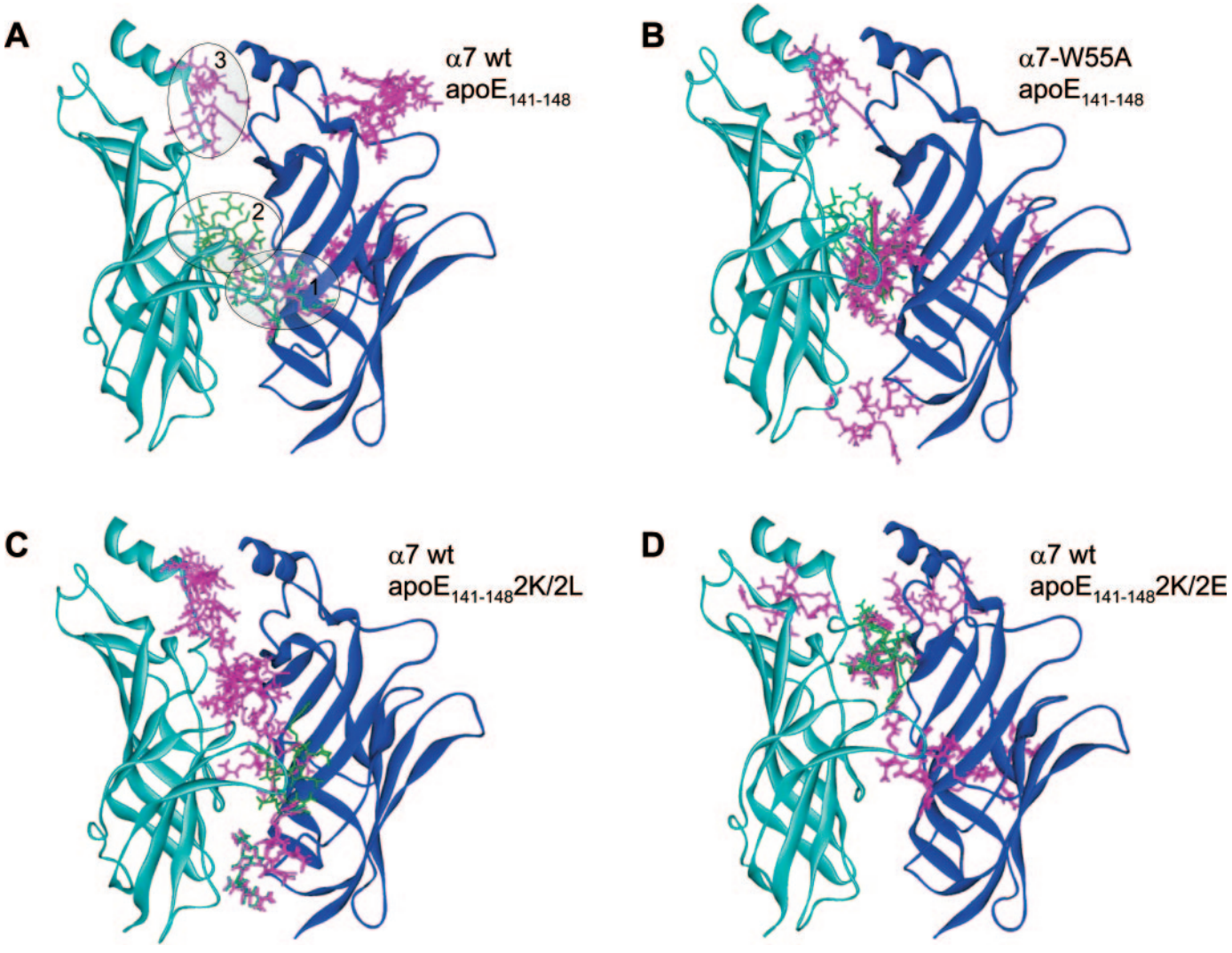

Fig. 6. Models of various apoE peptides docked between two α7 nAChR subunits. Pictured are the top 10 conformations of apoE$_{141–148}$ at the wild-type α7 nAChR (A), apoE$_{141–148}$ at the α7-W55A nAChR (B), apoE$_{141–148}$2K/2L at the wild-type α7 nAChR (C), and apoE$_{141–148}$2K/2E at the wild-type α7 nAChR (D). The top-ranked position is highlighted in dark green, whereas the second top position is in light green. ApoE$_{141–148}$ docking at both the wild-type and W55A mutant α7 nAChR suggested binding at three locations: 1) at the level of the C-loop at or near the ligand binding pocket, 2) just above the level of the C-loop on the pore side, and 3) near the α helix at the top of the receptor. The activity-dependant peptide apoE$_{141–148}$2K/2L suggests similar potential interactions with slightly more variable locations. The most favorable potential interactions for the inactive peptide, apoE$_{141–148}$2K/2E, are not located near Trp55. ApoE peptides were docked using ZDOCKpro.

near the ligand binding pocket (Corringer et al., 2000; Brejc et al., 2001; Celie et al., 2004; Young et al., 2007). Mutation of the homologous residue to Trp55 in related receptors has a variety of effects, including decreases in agonist and antagonist affinity and/or decreases in ACh potency (Corringer et al., 1995; Spier and Lummis, 2000; Xie and Cohen, 2001; Fruchart-Gaillard et al., 2002).

The combined experimental and computational data suggest that the interaction of apoE$_{141–148}$ and the α7 nAChR is dependent on Trp55, and occurs at the interface between two subunits at the level of the C-loop. Additional mutations of Trp55 to Cys, Val, Tyr, Phe, Leu, Thr, and Arg were used to test the importance of size, charge, polarity, and hydrophobicity of the position 55 side chain in the ability of apoE$_{141–148}$ to inhibit α7 nAChR responses. The finding that the W55R mutation was nonfunctional suggests that a positively charged side chain at position 55 disrupts channel gating, which could be due to a variety of mechanisms, including incorrect folding or trafficking of the protein and inability of ACh to bind and/or gate the receptor. The presence of both nonpolar (Trp, Phe, Val, Ala, Cys) and polar (Tyr) side-chains did not change the ability of apoE$_{141–148}$ to inhibit α7 nAChR signaling, suggesting that polarity of the side chain is not critical in the peptide/receptor interaction.

The preservation of the hydrophobic (and not just aromatic) nature of the amino acid at position 55 with Val, Cys, Phe, and Tyr suggests that the hydrophobicity of this position is key to the ability of apoE$_{141–148}$ to block ACh responses. Computational docking of apoE$_{141–148}$ with both the α7 nAChR and the α7-W55A nAChR also indicates that hydrophobic interactions between the three leucines of apoE$_{141–148}$ and the tryptophan at position 55 could be important to the peptide/receptor interaction. Although alanine is considered hydrophobic, the predicted loss of interaction with the leucines of apoE$_{141–148}$ is not surprising, considering both its low ranking on hydrophobicity scales and its smaller size (Nozaki and Tanford, 1971; Zamyatnin, 1972), indicating that both hydrophobicity and the size of the amino acid at position 55 are critical for the inhibition of ACh current responses by apoE$_{141–148}$.

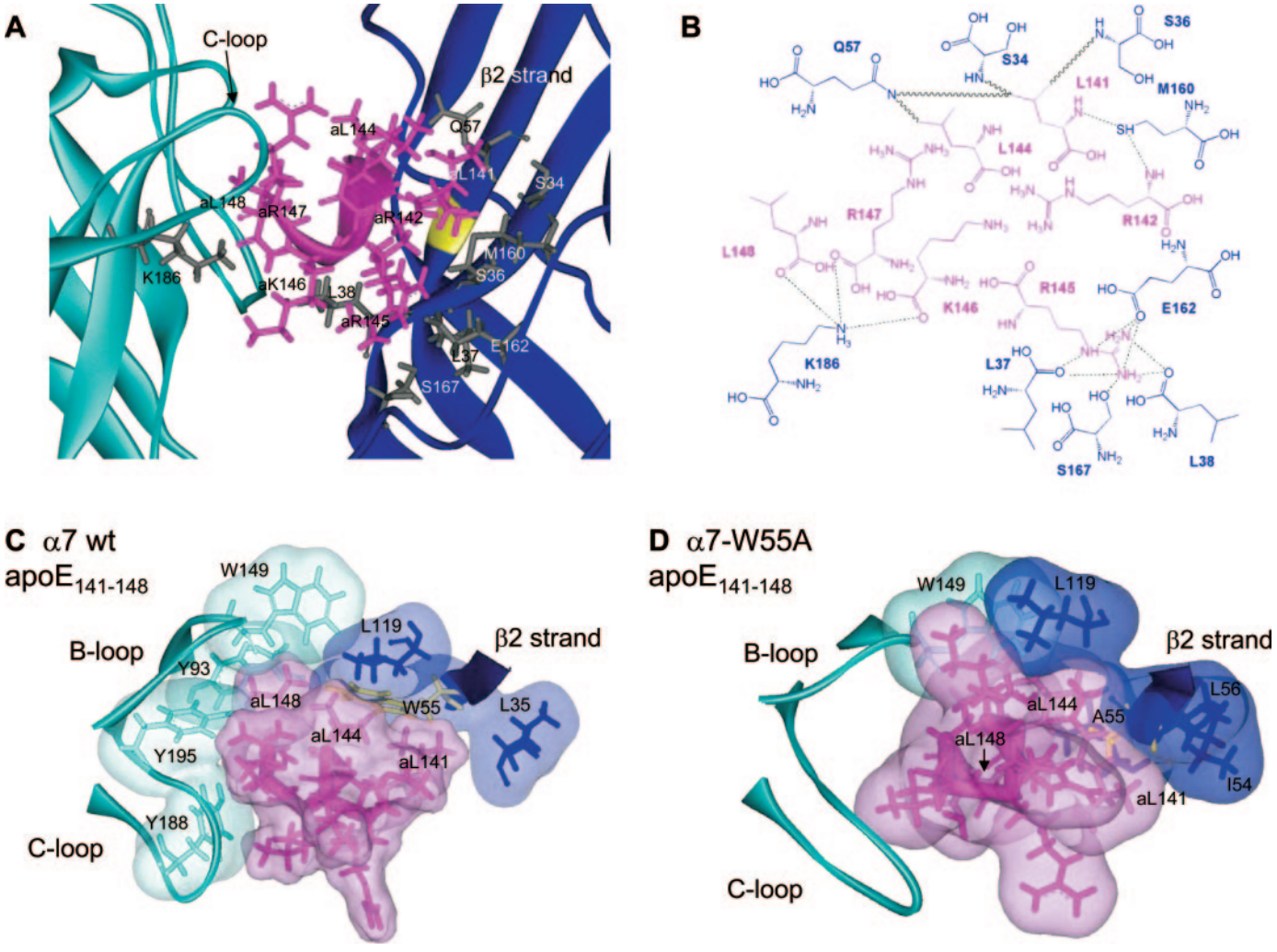

Fig. 7. Potential docking of apoE$_{141–148}$ to the wild-type α7 and α7-W55A nAChR. A, ApoE$_{141–148}$ docked to the wild-type α7 nAChR. Amino acids from the receptor that make potential hydrogen bonds or Van der Waals interactions with the peptide are shown in gray. The backbone of Trp55 is highlighted in yellow. ApoE$_{141–148}$ peptide amino acids are designated with a small "a". B, specific hydrogen bonds (dotted) and Van der Waals interactions (wavy) between residues in apoE$_{141–148}$ and α7 nAChR amino acids are illustrated schematically. They are enumerated along with distances in Table 2. Potential hydrophobic interaction for apoE$_{141–148}$ with the wild-type α7 nAChR (C), and α7-W55A nAChR (D) are highlighted. Each of the leucines in apoE$_{141–148}$ makes a possible hydrophobic contact with Trp55 (yellow) in the wild-type α7 receptor, whereas in the α7-W55A mutant, only one potential interaction between apoE Leu144 and Ala55 (yellow) remains.

The ^{125}I-α-BgTx binding data indicate that apoE$_{141–148}$ is noncompetitive at the α-BgTx binding site, similar to previous functional data suggesting the peptide and toxin were noncompetitive (Gay et al., 2006). This finding suggests that if apoE$_{141–148}$ is interacting directly with Trp55 and binding at the interface between two subunits at the level of the C-loop, the peptide is binding to a unique microdomain that does not exclude α-BgTx binding to the receptor. Recent crystal structure work has demonstrated that traditional noncompetitive nAChR ligands, such as galanthamine and cocaine, bind at the level of the C-loop and interact with aromatic amino acids within the ligand binding domain (Hansen and Taylor, 2007). However, these findings are with the heteromeric AChBP instead of a homomeric nAChR. As mentioned earlier, the binding data may also support the hypothesis that apoE$_{141–148}$ may be interacting with the α7 nAChR at a site remote from Trp55, and we cannot rule out the possibility that the loss of apoE peptide inhibition at the α7-W55A mutant receptor is due to a more global conformational change in the receptor.

Several additional peptide/receptor interactions are predicted from the molecular modeling. Some of these were tested functionally by single-point mutations of the α7 nAChR including: Ser34 with apoE Leu141, Glu184 with apoE Arg145, Trp149 with apoE Leu148, Lys208 with apoE Lys146 and Arg147, and Leu148. However, mutation of each of these amino acids to alanine did not block the ability of apoE$_{141–148}$ to inhibit ACh-mediated functional responses. These data are somewhat surprising; however, because each of these was a single-point mutation and because the peptide is predicted to make multiple contacts with the receptor, it could be that the loss of one of these individual interactions is not enough to disrupt the functional effects of apoE$_{141–148}$. These findings might also suggest that the hydrophobic interaction between the apoE peptide and Trp55 may be particularly critical to the peptide's ability to block α7 nAChR function.

ApoE$_{141–148}$2K/2L demonstrated activity-dependent block of α7 nAChR function at both the wild-type and the α7-W55A mutant receptors. The current data suggest that the vast majority of block by apoE$_{141–148}$2K/2L at α7-W55A nAChRs was activity-dependent (> 90%), whereas ~75% of the block at wild-type α7 nAChRs was activity-dependent. This is in contrast to apoE$_{141–148}$, which undergoes activity-*independent* block of α7 nAChRs (Gay et al., 2006). In addition, apoE$_{141–148}$2K/2L inhibition of α7 nAChRs is voltage-independent, indicating that this activity-dependent peptide is most likely not acting as an open channel blocker and is binding somewhere within the extracellular portion of the receptor.

When the overall pattern of the top 25 ranked peptide/receptor interactions are considered for apoE$_{141–148}$2K/2L, this mutated apoE peptide demonstrated a much broader range of suggested interaction sites than apoE$_{141–148}$. Although some of the predicted docking sites include Trp55, others are at the interface between the two subunits but removed from Trp55. This spread may indicate why the functional activity of apoE$_{141–148}$2K/2L at the α7 nAChR was different from apoE$_{141–148}$. However, the docked peptide conformer position with the least energy was similar in location to the apoE$_{141–148}$ peptide-docked position. This supports the experimental observation that apoE$_{141–148}$2K/2L preserves the majority of nAChR inhibition with a slightly different mechanism of blockade. Both the modeling and functional data suggest that apoE$_{141–148}$ and apoE$_{141–148}$2K/2L may have unique modes of interaction with α7 nAChRs that partially overlap.

Characterization of the mutated α7 nAChRs revealed that the majority of functional mutations demonstrated slight to moderate increases or decreases in ACh potency. For the majority of mutant α7 nAChRs, there is an increase in Hill slope (while a few have decreases), suggesting that these mutations may cause a change in either the cooperativity of binding and/or the cooperativity of gating the receptor

TABLE 2
Potential molecular interactions between apoE$_{141–148}$ and the α7 nAChR

apoE$_{141–148}$	α7 nAChR	Subunit	Potential Interaction	Distance
				Å
L141	Ser34[a]	Complementary	VDW	3.3
L141	Leu35	Complementary	Hydrophobic	4.0
L141	Ser36	Complementary	VDW	3.0
L141	Trp55[a]	Complementary	Hydrophobic	3.3
L141	Gln57	Complementary	VDW	3.1
L141	Leu119	Complementary	Hydrophobic	3.1
L141	Met160	Complementary	H bond	2.7
R142	Met160	Complementary	H bond	2.7
L144	Trp55[a]	Complementary	Hydrophobic	3.7
L144	Gln57	Complementary	VDW	2.7
R145	Leu37	Complementary	H bond	2.0/2.8
R145	Leu38	Complementary	H bond	2.6/2.7
R145	Glu162[a]	Complementary	H bond	2.2/2.9/2.9
R145	Ser167	Complementary	H bond	2.9
K146	Lys186[a]	Principal	H bond	2.4
R147	Lys186[a]	Principal	H bond	1.8
L148	Trp55[a]	Complementary	Hydrophobic	1.6
L148	Tyr93	Principal	Hydrophobic	4.3
L148	Trp149[a]	Principal	Hydrophobic	3.0
L148	Lys186[a]	Principal	H bond	3.6
L148	Tyr188[a]	Principal	Hydrophobic	4.5
L148	Tyr195[a]	Principal	Hydrophobic	3.3

VDW, van der Waals.
[a] Amino acid was mutated to alanine in the current study.

(Colquhoun, 1998). High-affinity desensitization could affect dose-response curves, causing them to appear steeper than in reality; in contrast, however, fast desensitization of α7 nAChRs may clip the true peak amplitude, leading to an underestimate of the Hill coefficient. Differences in maximal ACh responses between mutant receptors were not compared because of variations in peak current from day to day and across batches of oocytes, as well as possible disparities in receptor expression levels. Several of the single-point mutations resulted in nonfunctional channels. It was not determined whether these mutant receptors were nonfunctional because they were not expressed, because they could not bind ACh, or because the channel could not be gated. However previously, similar mutations in the chick α7 nAChR for W55R, D89K, Y188A, E193K, and Y195A resulted in channels that were expressed in human embryonic kidney 293 cells and bound α-bungarotoxin (Fruchart-Gaillard et al., 2002).

Other naturally occurring small peptides are known to inhibit nAChR activity, including the heavily studied conotoxins. The small α-conotoxin ImI selectively binds $\alpha7/\alpha2\beta3$-containing nAChRs. Independent crystal structures of this peptide have recently been solved with the *A. californica* AChBP (Hansen et al., 2005; Ulens et al., 2006). This α-helical peptide interacts at the interface between two subunits near the ACh binding site, similar to the proposed interaction site of apoE$_{141–148}$. Some of the contacts described in the crystal structures are similar to those for the apoE peptide, including interactions with most of the aromatic amino acids within the ligand binding pocket (Ac-AChBP Tyr91, Trp145, Tyr186, and Tyr193). Although both crystal structures indicate that AChBP Tyr55 is near the binding site for this α-conotoxin, neither suggests a stabilizing interaction between Tyr55 and the peptide. This is in contrast to the functional and modeling data presented for apoE$_{141–148}$, which predicts a key role for Trp55 in peptide inhibition of ACh responses. However, the interaction between α7 nAChRs and apoE$_{141–148}$ seems distinct from that for α-conotoxin ImI because the former does not compete for α-bungarotoxin binding, whereas the latter is competitive (Ellison et al., 2003; Gay et al., 2006).

The therapeutic potential of apoE mimetic peptides in a variety of disease states has been demonstrated, including: improved cognitive recovery after head injury and ischemia, as well as decreasing symptoms in an animal model of multiple sclerosis (Lynch et al., 2005; McAdoo et al., 2005; Li et al., 2006). The therapeutic effects of apoE mimetic peptides are thought to occur through an anti-inflammatory mechanism (Laskowitz et al., 2006). It is noteworthy that α7 nAChRs are expressed peripherally in immune cells, where they are thought to play a role in the suppression of the pro-inflammatory cytokine, tumor necrosis factor (Pavlov and Tracey, 2006). However, activation, not inhibition, of α7 nAChR seems key to this anti-inflammatory response. The current findings may have considerable implications in the development of novel therapeutics through the use of apoE-derived peptides to regulate nAChR signaling in terms of understanding both the potential mechanism of action and possible side effects of the peptides.

In conclusion, the current study engaged both physiological and molecular modeling data to characterize the probable structure/function relationship between an apoE peptide and the α7 nAChR. These data suggest that hydrophobic interactions between apoE$_{141–148}$ and the α7 nAChR are key to peptide inhibition of receptor function. In addition, this study identifies for the first time an activity-dependent antagonist for α7 nAChRs, the apoE$_{141–148}$2K/2L peptide, which may interact with α7 nAChRs in a manner somewhat different from apoE$_{141–148}$. The current findings propose a mode for apoE peptide binding that directly blocks α7 nAChR activity, and therefore may disrupt normal nAChR signaling both in the peripheral and central nervous system.

Acknowledgments

We thank L. Pedersen and S. Gentile for advice in preparing the manuscript.

References

Berg DK and Conroy WG (2002) Nicotinic alpha 7 receptors: synaptic options and downstream signaling in neurons. *J Neurobiol* **53:**512–523.
Brejc K, van Dijk WJ, Klaassen RV, Schuurmans M, van Der Oost J, Smit AB, and Sixma TK (2001). Crystal structure of an ACh-binding protein reveals the ligand-binding domain of nicotinic receptors. *Nature* **411:**269–276.
Celie PH, Kasheverov IE, Mordvintsev DY, Hogg RC, van Nierop P, van Elk R, van Rossum-Fikkert SE, Zhmak MN, Bertrand D, Tsetlin V, et al. (2005a) Crystal structure of nicotinic acetylcholine receptor homolog AChBP in complex with an alpha-conotoxin PnIA variant. *Nat Struct Mol Biol* **12:**582–588.
Celie PH, Klaassen RV, van Rossum-Fikkert SE, van Elk R, van Nierop P, Smit AB, and Sixma TK (2005b) Crystal structure of acetylcholine-binding protein from Bulinus truncatus reveals the conserved structural scaffold and sites of variation in nicotinic acetylcholine receptors. *J Biol Chem* **280:**26457–26466.
Celie PH, van Rossum-Fikkert SE, van Dijk WJ, Brejc K, Smit AB, and Sixma TK (2004) Nicotine and carbamylcholine binding to nicotinic acetylcholine receptors as studied in AChBP crystal structures. *Neuron* **41:**907–914.
Chen R, Li L, and Weng Z (2003) ZDOCK: an initial-stage protein-docking algorithm. *Proteins* **52:**80–87.
Clay MA, Anantharamaiah GM, Mistry MJ, Balasubramaniam A, and Harmony JA (1995) Localization of a domain in apolipoprotein E with both cytostatic and cytotoxic activity. *Biochemistry* **34:**11142–11151.
Colquhoun D (1998) Binding, gating, affinity and efficacy: the interpretation of structure-activity relationships for agonists and of the effects of mutating receptors. *Br J Pharmacol* **125:**924–947.
Corringer PJ, Galzi JL, Eisele JL, Bertrand S, Changeux JP, and Bertrand D (1995) Identification of a new component of the agonist binding site of the nicotinic α7 homooligomeric receptor. *J Biol Chem* **270:**11749–11752.
Corringer PJ, Le Novère N, and Changeux JP (2000) Nicotinic receptors at the amino acid level. *Annu Rev Pharmacol Toxicol* **40:**431–458.
Dutertre S and Lewis RJ (2006) Toxin insights into nicotinic acetylcholine receptors. *Biochem Pharmacol* **72:**661–670.
Ellison M, McIntosh JM, and Olivera BM (2003) α-Conotoxins ImI and ImII. Similar α7 nicotinic receptor antagonists act at different sites. *J Biol Chem* **278:**757–764.
Fruchart-Gaillard C, Gilquin B, Antil-Delbeke S, Le Novère N, Tamiya T, Corringer PJ, Changeux JP, Menez A, and Servent D (2002) Experimentally based model of a complex between a snake toxin and the alpha 7 nicotinic receptor. *Proc Natl Acad Sci U S A* **99:**3216–3221.
Gay EA, Klein RC, and Yakel JL (2006) Apolipoprotein E-derived peptides block alpha7 neuronal nicotinic acetylcholine receptors expressed in *Xenopus* oocytes. *J Pharmacol Exp Ther* **316:**835–842.
Hansen SB, Sulzenbacher G, Huxford T, Marchot P, Bourne Y, and Taylor P (2006) Structural characterization of agonist and antagonist-bound acetylcholine-binding protein from *Aplysia californica*. *J Mol Neurosci* **30:**101–102.
Hansen SB, Sulzenbacher G, Huxford T, Marchot P, Taylor P, and Bourne Y (2005) Structures of *Aplysia* AChBP complexes with nicotinic agonists and antagonists reveal distinctive binding interfaces and conformations. *EMBO J* **24:**3635–3646.
Hansen SB and Taylor P (2007) Galanthamine and non-competitive inhibitor binding to Ach-binding protein: evidence for a binding site on non-alpha-subunit interfaces of heteromeric neuronal nicotinic receptors. *J Mol Biol* **369:**895–901.
Holm L and Park J (2000) DaliLite workbench for protein structure comparison. *Bioinformatics* **16:**566–567.
Holm L and Sander C (1995) Dali: a network tool for protein structure comparison. *Trends Biochem Sci* **20:**478–480.
Jones S, Sudweeks S, and Yakel JL (1999) Nicotinic receptors in the brain: correlating physiology with function. *Trends Neurosci* **22:**555–561.
Klein RC and Yakel JL (2004) Inhibition of nicotinic acetylcholine receptors by apolipoprotein E-derived peptides in rat hippocampal slices. *Neuroscience* **127:**563–567.
Laskowitz DT, Fillit H, Yeung N, Toku K, and Vitek MP (2006) Apolipoprotein E-derived peptides reduce CNS inflammation: implications for therapy of neurological disease. *Acta Neurol Scand Suppl* **185:**15–20.
Laskowski RA, MacArthur MW, Moss DS, and Thornton JM (1993) PROCHECK: A program to check the sterochemical quality of protein structures. *J Appl Crystallogr* **26:**283–291.
Le Novère N, Grutter T, and Changeux JP (2002) Models of the extracellular domain of the nicotinic receptors and of agonist- and Ca^{2+}-binding sites. *Proc Natl Acad Sci U S A* **99:**3210–3215.

Levin ED (2002) Nicotinic receptor subtypes and cognitive function. *Journal of Neurobiology* **53:**633–640.
Li FQ, Sempowski GD, McKenna SE, Laskowitz DT, Colton CA, and Vitek MP (2006) Apolipoprotein E-derived peptides ameliorate clinical disability and inflammatory infiltrates into the spinal cord in a murine model of multiple sclerosis. *J Pharmacol Exp Ther* **318:**956–965.
Li L, Chen R, and Weng Z (2003) RDOCK: refinement of rigid-body protein docking predictions. *Proteins* **53:**693–707.
Lynch JR, Wang H, Mace B, Leinenweber S, Warner DS, Bennett ER, Vitek MP, McKenna S, and Laskowitz DT (2005) A novel therapeutic derived from apolipoprotein E reduces brain inflammation and improves outcome after closed head injury. *Exp Neurol* **192:**109–116.
Marques MA, Tolar M, Harmony JA, and Crutcher KA (1996) A thrombin cleavage fragment of apolipoprotein E exhibits isoform-specific neurotoxicity. *Neuroreport* **7:**2529–2532.
McAdoo JD, Warner DS, Goldberg RN, Vitek MP, Pearlstein R, and Laskowitz DT (2005) Intrathecal administration of a novel apoE-derived therapeutic peptide improves outcome following perinatal hypoxic-ischemic injury. *Neurosci Lett* **381:** 305–308.
Morris AL, MacArthur MW, Hutchinson EG, and Thornton JM (1992) Stereochemical quality of protein structure coordinates. *Proteins* **12:**345–364.
Nozaki Y and Tanford C (1971) The solubility of amino acids and two glycine peptides in aqueous ethanol and dioxane solutions. Establishment of a hydrophobicity scale. *J Biol Chem* **246:**2211–2217.
Pavlov VA and Tracey KJ (2006) Controlling inflammation: the cholinergic anti-inflammatory pathway. *Biochem Soc Trans* **34:**1037–1040.
Picciotto MR and Zoli M (2002) Nicotinic receptors in aging and dementia. *J Neurobiol* **53:**641–655.
Raggenbass M and Bertrand D (2002) Nicotinic receptors in circuit excitability and epilepsy. *J Neurobiol* **53:**580–589.
Segelke BW, Forstner M, Knapp M, Trakhanov SD, Parkin S, Newhouse YM, Bellamy HD, Weisgraber KH, and Rupp B (2000) Conformational flexibility in the apolipoprotein E amino-terminal domain structure determined from three new crystal forms: implications for lipid binding. *Protein Sci* **9:**886–897.
Sine SM (2002) The nicotinic receptor ligand binding domain. *J Neurobiol* **53:**431–446.
Spier AD and Lummis SC (2000) The role of tryptophan residues in the 5-Hydroxytryptamine(3) receptor ligand binding domain. *J Biol Chem* **275:**5620–5625.
Tolar M, Marques MA, Harmony JA, and Crutcher KA (1997) Neurotoxicity of the 22 kDa thrombin-cleavage fragment of apolipoprotein E and related synthetic peptides is receptor-mediated. *J Neurosci* **17:**5678–5686.
Ulens C, Hogg RC, Celie PH, Bertrand D, Tsetlin V, Smit AB, and Sixma TK (2006) Structural determinants of selective alpha-conotoxin binding to a nicotinic acetylcholine receptor homolog AChBP. *Proc Natl Acad Sci U S A* **103:**3615–3620.
Unwin N (2005) Refined structure of the nicotinic acetylcholine receptor at 4A resolution. *J Mol Biol* **346:**967–989.
Wiehe K, Pierce B, Mintseris J, Tong WW, Anderson R, Chen R, and Weng Z (2005) ZDOCK and RDOCK performance in CAPRI rounds 3, 4, and 5. *Proteins* **60:**207–213.
Xie Y and Cohen JB (2001) Contributions of Torpedo nicotinic acetylcholine receptor gamma Trp-55 and delta Trp-57 to agonist and competitive antagonist function. *J Biol Chem* **276:**2417–2426.
Young GT, Broad LM, Zwart R, Astles PC, Bodkin M, Sher E, and Millar NS (2007) Species selectivity of a nicotinic acetylcholine receptor agonist is conferred by two adjacent extracellular β4 amino acids that are implicated in the coupling of binding to channel gating. *Mol Pharmacol* **71:**389–397.
Zamyatnin AA (1972) Protein volume in solution. *Prog Biophys Mol Biol* **24:**107–123.

Address correspondence to: Jerrel L. Yakel, NIEHS, F2-08, P.O. Box 12233, 111 T. W. Alexander Drive, Research Triangle Park, NC 27709. E-mail: yakel@niehs.nih.gov